ANNALS OF GEOPHYSICS, 67, 5, A554, 2024, doi:10.4401/ag-9073
OPEN ACCESS

Detection of infrasound sources using three-years array data in 2019-2021 deployed at the Lützow-Holm Bay region, Antarctica

Masaki Kanao[*,1], Takahiko Murayama[2], Masa-Yuki Yamamoto[3], Yoshiaki Ishihara[4], Dan Muramatsu[5], Makiko Iwakuni[2], Mami Nogami[2]

(1) National Institute of Polar Research, Research Organization of Information and Systems, Midori-cho, Tachikawa-shi, Tokyo
(2) Japan Weather Association, Sunshine 60 Bldg. 55F Higashi-Ikebukuro, Toshima-ku, Tokyo, Japan
(3) Kochi University of Technology, 185 Miyanokuchi, Tosayamada-cho, Kami-shi, Kochi, Japan
(4) Japan Aerospace Exploration Agency, Sengen 2-1-1, Tsukuba, Ibaraki 305-8505, Japan
(5) Earthquake Research Institute, The University of Tokyo, 1-1-1, Yayoi, Bunkyo-ku, Tokyo, Japan

Article history: received February 5, 2024; accepted November 15, 2024

Abstract

Time-space variations of infrasound source locations for three years, 2019-2021, were studied by using a combination of two local arrays in the Lützow-Holm Bay region (LHB), Antarctica. The local arrays deployed at two coastal outcrops clearly detected temporal variations in signal frequency content as well as propagating directions during the three years. A large number of infrasound sources were detected with many located to the north and north-west directions from the arrays. These events were generated within the Southern Indian Ocean and the northern part of LHB with frequency-content of a few seconds; these "microbaroms" are believed to originate from oceanic swells. From austral summer to fall additional infrasound sources are determined to be located to the north-east. These sources might be related to the effects of katabatic winds across the continental coastal area. Furthermore, several impulsive infrasound events during the winter had higher predominant frequencies of a few Hz, higher than the microbaroms. On the basis of a comparison of source locations with sea-ice and glacier distribution form MODIS satellite images, these high-frequency sporadic sources may be cryo-seismic signals associated with cryosphere dynamics near the local arrays. These results suggest that infrasound waves can be used to monitor surface environments in the coastal area of Antarctica.

Keywords: Infrasound; Array analysis; Lützow-Holm Bay; Antarctic coast; Cryosphere dynamics; Katabatic wind; Microbaroms

1. Introduction

"Infrasound" signals are sub-audible pressure waves with frequency from the cut-off of a sound (3.21 mHz, for a 15°C isothermal atmosphere) to the lowest of the human audible band (20 Hz) which can propagate in the

atmosphere for several thousand kilometers and recorded at the Earth's surface when excited by large energy sources (Hedlin et al., 2002). There are many infrasound sources including tsunamis, volcanic eruptions, ocean waves, earthquakes, aircraft, thunder, sprites, fireballs, meteorite falls, reentry of artificial vehicles and aurora activities (Arai et al., 2011; Iyemori et al., 2005; Matoza et al., 2007; Arrowsmith et al., 2008; Wilson, 1969). Infrasound can also be used to constrain physical aspects of the atmosphere such as temperature and wind profiles. In polar regions, such as Antarctica, temporal and spatial variations in atmospheric pressure are generated by physical interactions between atmosphere, oceans, cryosphere, and solid earth. Dynamic changes of surface environments can excite infrasound waves that can be measured by instruments deployed in polar regions. Podolskiy et al. (2017) conducted simultaneous observation using seismic and infrasound sensors at Bowdoin Glacier in Greenland. They validated infrasound sources using ground-based time-lapse cameras to better localize small size sources like calving events.

In April 2008, infrasound observations from a single sensor were started at the Japanese main station; Syowa (SYO; 69.0S, 39.6E), in the Lützow-Holm Bay (LHB) of Antarctica (Yamamoto et al., 2013). Previously, long-term monitoring of infrasound had been conducted at two permanent International Monitoring System infrasound arrays in Antarctica operated by USA (Station; IS55) and by Germany (Station IS27). After five years of observations using the single sensor at SYO (Ishihara et al., 2015), the single sensor was replaced by a tripartite array during austral summer of 2013 (Murayama et al., 2015). Eleven years of infrasound data and results at SYO (in 2008 to 2019) were published in the Polar Data Journal (Ishihara et al., 2020). Long-term variability of the frequency content of the data were documented over the eleven seasons with the background contamination by signals of oceanic swells (microbaroms).

In addition to the local array at SYO, several field stations with infrasound sensors were established along the eastern coast of LHB beginning in the austral summer of 2013 (Murayama et al., 2015). Additional local arrays with different sensor offsets were deployed in parallel with SYO; a second array was established over the continental ice sheet (S16; 68.1S, 41.8E) near the eastern coast of LHB. Detail of the observation system for these arrays and initial data recorded in austral summer of 2013 were previously reported (Murayama et al., 2015). These data documented the frequency content and source azimuth associated with microbaroms from Southern Indian Ocean for fifty days during the in austral summer in 2013. Using the array deployed at LHB, infrasound signals were associated with seven identical events in 2015 (Murayama et al., 2017a). Many of the sources were assumed to have cryoseismic origins; ice-quakes associated with calving of glaciers, discharge of sea-ice, collision between sea-ice and icebergs around the region.

The long-term variability of infrasound source locations for eight months in January-August 2015 were investigated using the two arrays deployed at SYO and S16 (Murayama et al., 2017b). Source mechanisms of these events were associated with cryosphere dynamics surrounding LHB. The study focused on events occurring in mid-April 2015 associated with the discharge of a large volume of sea-ice, together with collision events involving icebergs surrounding LHB which had drifted eastward from Enderby Land offshore. Similar sea-ice discharge events at LHB in April 2016 were estimated to be associated with the dynamics of fragmentation of sea-ice and ice-bergs (Murayama et al., 2018). Recently, the migration of source locations and associated arrival orientations of infrasound signals in the same area were documented from January to April 2017 (Murayama et al., 2023).

In the austral summer of 2018 and 2019, the array on the continental ice sheet (S16) was moved to a new outcrop (Langhovde (LNG); 69.1S, 39.4E) about 20 km to the south of SYO along the east coast of LHB (Fig. 1). On the basis of these new infrasound observations and research history in LHB, time-space variations of infrasound source locations for 2019-2021 are investigated in detail using the two local arrays, SYO and LNG, deployed at outcrops along the east coast of LHB. Temporal variations in frequency content together with array estimated propagation directions are documented for the two local arrays and interpretated in terms of dynamic processes in the surface environment in the area.

2. Array observation and analytic procedure

A total of nine infrasound instruments were deployed along the eastern coast of LHB in January of 2013 and 2014 (Murayama et al., 2015). Two triangle arrays were deployed at SYO (with a 100 m spacing triangle) and near S16 on the continental ice sheet (with a 1 km spacing triangle), which is 15 km east of SYO (Fig. 1). In addition to these arrays, isolated single stations were deployed at three outcrops along the coast of LHB (i.e., Langhovde (LNG), Skallen (SKL) and Rundvagshetta (RDV)). This station network on LHB, consisted of multi-scale array configurations

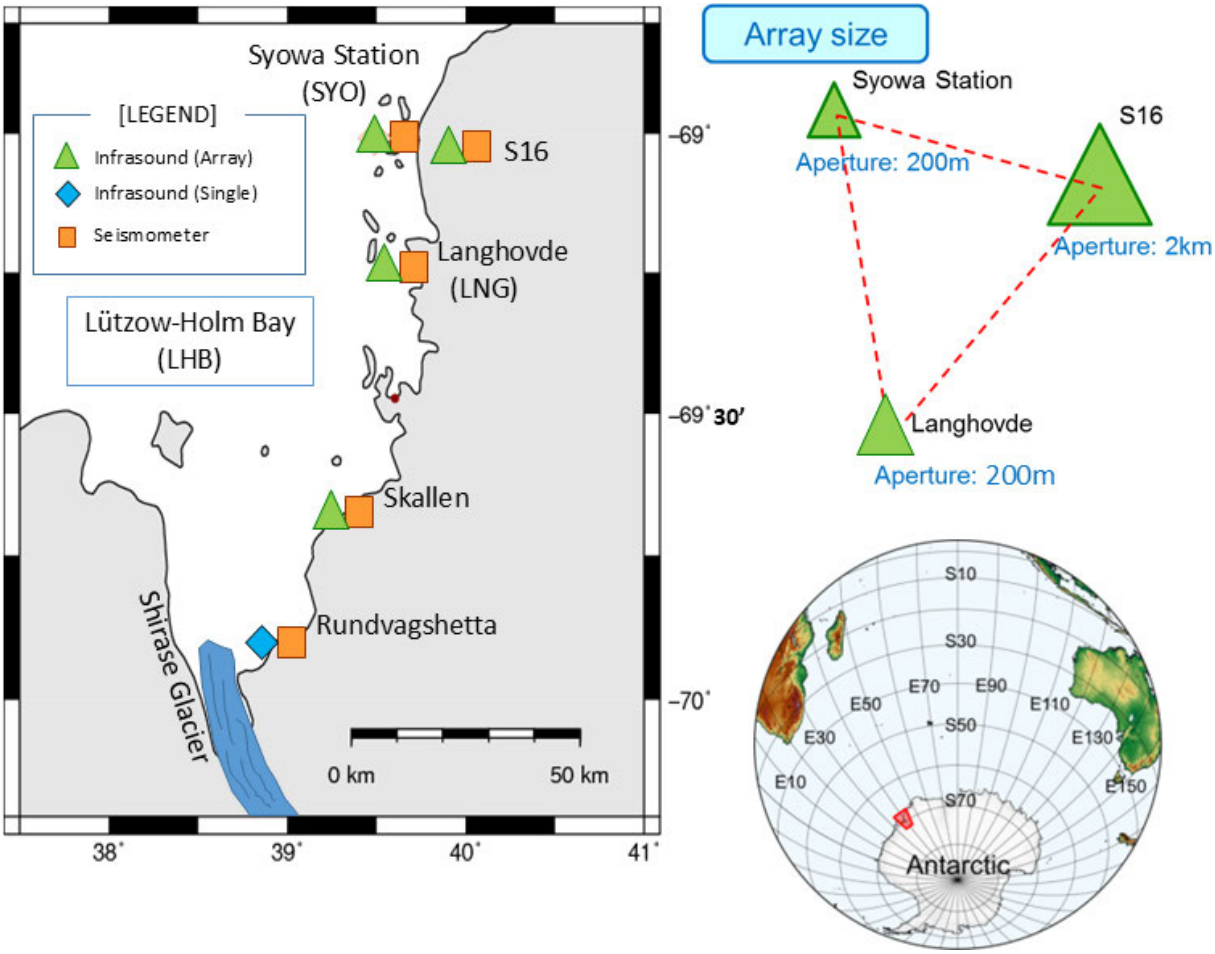

Figure 1. (left) Location map of the infrasound array deployment in the Lützow-Holm Bay region (LHB), Antarctica, for the period in 2019-2021. Array stations of infrasound (green triangles), single stations of infrasound (blue diamond) and broadband seismometers (orange squares) are respectively indicated. (upper right) Array configuration of infrasound stations to localize the source signals. Tripartite arrays had been deployed by the aperture size in 200 m at both the Syowa Station (SYO) and other outcrop station at Langhovde (LNG). The two stations are 20 km from each other.

and is used to detect signals by identifying different wavelengths with corresponding frequencies for each array depending on its size (Fig. 1).

Array observations on the continental ice sheet (S16) were terminated in January of 2018 and moved to a new outcrop (LNG; 69.1S, 39.4E; with a 100 m spacing triangle) about 20 km south of SYO along the east coast of LHB in January of 2019. The infrasound sensors on the ice sheet at S16 had been gradually buried under the snow/ice accumulation during the last few years after the beginning of the observation in 2013. The new array location was moved to the ice-free outcrop area at LHB, with similar surface environmental conditions like SYO. Most of the outcrop stations also included broadband seismometers (Guralp Systems CMG-40T; for details see Kanao et al., 2011) in order to compare the seismic and infrasound signals across similar frequency bands.

Chaparral Physics Model 25 micro-barometer (developed by the University of Alaska, USA, with a detectable frequency range of 0.1-200 Hz) were deployed at most stations except for SKL (SAYA Co., INF03 type). Hose arrays were used to reduce wind noise acting as mechanical low-pass filters (Walker and Hedlin, 2010; Hedlin and Alcoverro, 2005). Multiply (eight) connected porous hoses were used at the SYO array. A single-hose was used at all the other field stations to reduce installation efforts. The porous hoses were buried beneath mounds of stones/snow-ice collected from around the observation sites to reduce the vibration effect of strong winds. Information on the specification of the infrasound sensors and array configurations of SYO and LNG are summarized in Table 1a and 1b. Moreover, detail configurations of the observation system (power supply, data acquisition and transmission) are included in Murayama et al. (2015).

(a) **Specifications of the Infrasound Sensor and Sampling**

Item	Specification
Model	Chaparral Physics Model 25
Sensitibity	2.0 volts/Pascal (1 Hz, 0-20 Pa full scale range)
Frequency range	0.1-200 Hz
Resolution	Several mPa
Acoustic inlet(s)	4-port manifold inlet on bottom
Output type	True differential output
Sampling rate	1-100 Hz
	

(b) **Specifications of the Infrasound Array**

Item	Specification	
	SYO	LNG
Array type	Tripartite array	Tripartite array
Number of elements	3	3
Aperture	approx. 200 m	approx. 140 m
Wind noise reducing system	Material: porous hose Configuration: 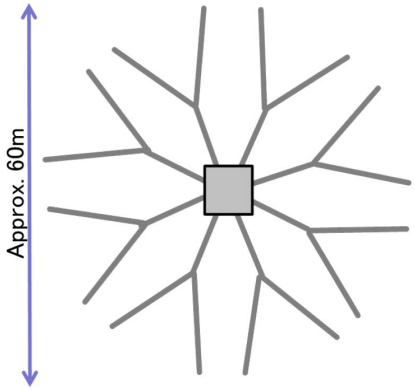	Material: porous hose Configuration: 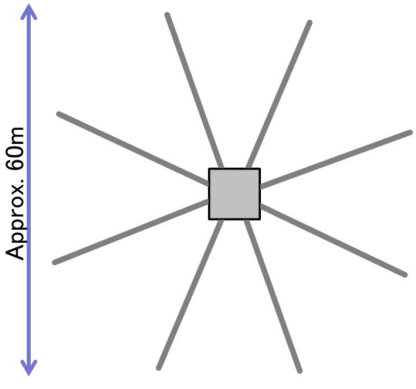

Table 1. Detailed specification of infrasound sensors (a) and arrays' configuration (b) deployed at SYO and LNG.

In order to estimate the propagation directions and event source locations of the infrasound signals, a two-step approach was adopted; the first step was to generate a bulletin for each array using the progressive multi-channel correlation (PMCC) algorithm (Cansi, 1995; Cansi and Klinger, 1997). Parameter settings in used PMCC and their related error estimations are summarized in Table 2; the second step was to associate signals from different arrays and provide source location as outputs as documented in the flowchart shown in Fig. 2 (which starts with two bulletins of the two arrays in LHB). One bulletin was for the SYO array (station ID; C1, C2 and C3) and the other was the LNG array (station ID; L1, L2, L3) (Fig. 1). As the array at SKL used different type sensors (SAYA Co., INF03; short period range covering with a low S/N ratio,), we did not utilize the SKL data to the PMCC analysis. A basic flow of the array analysis (Fig. 2) is summarized as follows: 1) Search for pairs of signals within ± 80 s of detected time difference on the basis of the bulletin dataset for the two arrays with the distance between the two arrays about 20 km; 2) Calculate a crossing point by spherical triangle method using the two estimated backazimuths for each array; 3) Set the candidate origin as grids around the cross point within ± 5 deg. range (as the error assumption of PMCC results), followed by calculating the averaged origin time and select the most probable grid; 4) Use calculated each celerity within the range of (between 0.28 km/s and 0.36 km/s) for both arrays, then output a final result.

PMCC setting

Item	Setting
Frequency band (Hz)	0.05-49.0 *The 0.05 to 49.0 Hz frequency band is divided into 10 logarithmic divisions.
Window Length (s)	30
Time Step (s)	3
Threshold Consistency (s)	0,1
Threshold FamMin	5
Threshold Distance	1
Sigma_Time (s)	6
Sigma_Freq (% of Nb bands)	5
Sigma_Speed (%)	20
Sigma_Azimuth (%)	10

Table 2. Actual PMCC software settings and their related error estimations.

Assuming a sound speed of 0.3 km/s in the lower atmosphere in the LHB area, origin times of all candidate crosses obtained within ± 5 degrees of the backazimuth of each array are determined from the arrival time of the signal in each array and each distances between the cross and the array. The cross with the minimum time difference between the origin times derived from each of the arrays is the most probable grid. Next, using the most probable grid, if the celerity is calculated within the range 0.28 km/s to 0.36 km/s, the origin is output. Therefore, if the real sound speed is apart than 0.3 km/s, or if the backazimuth from PMCC result has some error, it will affect the origin time and the source position.

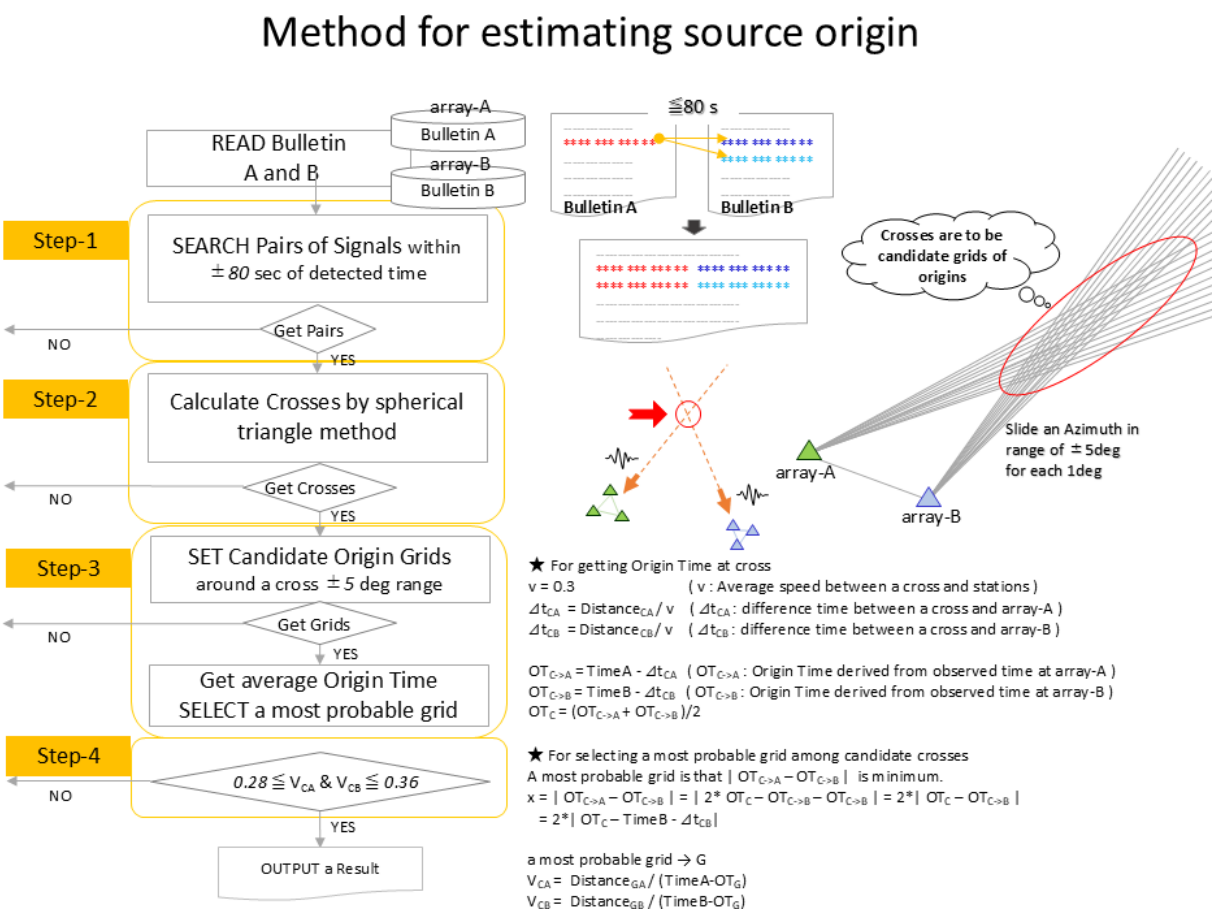

Figure 2. Flow chart of methodology to estimate the source locations and occurring times using each bulletin from PMCC (the Progressive Multi-Channel Correlation) for two infrasound arrays respectively. Detail procedures of each "Step" are described in the main text.

3. Azimuthal variations and frequency contents

Time series of azimuthal variations in arrival orientation and frequency contents of the detected infrasound signals using PMCC are shown in Figs. 3-5 covering the three years of 2019-2021. The vertical axis on the left hand side for all figures documents back-azimuth (from the station to the source orientation) for the two arrays. The color bar on right hand side of the panel of a year correspond to the central frequency [Hz] for each detected event (upper; liner-colored plot, lower; log-colored plot). Vacant times represent periods where the array analyses did not detect infrasound signals in each panel correspond to time windows with over 15 m/s wind speed, as observed at SYO (reported by the Japanese Meteorological Agency; JMA).

The two arrays produce similar variations in time of occurrence and backazimuth in the estimated source location over the three years, regardless of the fact that the two arrays are located 20 km apart along the East coast of LHB. Array estimates for LNG have relatively better S/N ratio because of decreased strong winds caused by storms particularly during the winter season. Longer-time continuous data were able to be analyzed at LNG during the extreme stormy condition with wind speed over 15 m/s. This extended analysis is a result of the location of LNG far from Southern Indian Ocean, where storms pass from west to east over the northern part of LHB.

The two outcrop arrays, LNG and SYO, along the East coast of LHB were found to have a more effective configuration for source detection than S16 on the ice sheet, because (Murayama et al., 2015; 2017): 1) the majority of sources were distributed to the northwest inside the LHB or Southern Ocean; 2) smaller aperture of the arrays (about 200 m) used to detect coherent source signals; 3) efficiency of multiple-connected porous hoses in noise reduction particular at SYO; 4) and relatively small S/N ratio on the outcrops (SYO and LNG) compared to the array on ice sheet (S16), because the ice sheet is affected by softer ground motions than the hard rock surface of the outcrop area.

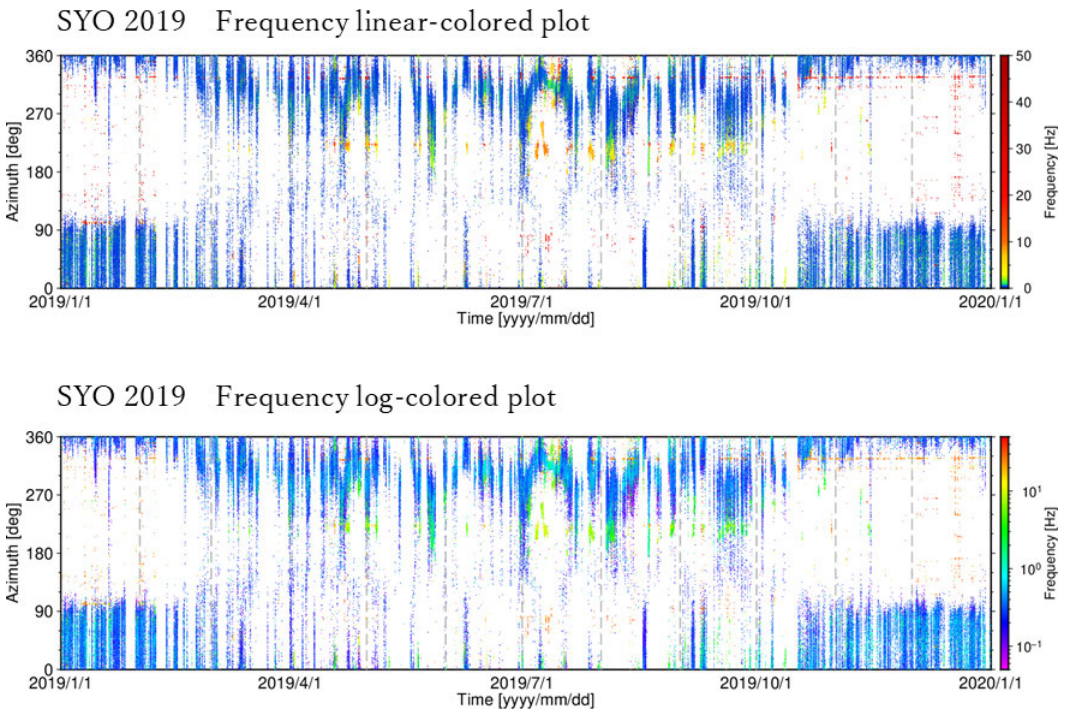

Figure 3a. Time sequence of azimuthal variation in arrival orientation and frequency contents of the detected infrasound signals by PMCC analysis (from January 01 to December 31, 2019, represented by a single year panel). The vertical axis for each panel indicates the back-azimuth (station-to-source) directions for SYO array. Colored bars representing in right hand side for each panel correspond to the central frequency [Hz] for each detected source event (upper; linear-colored plot, lower; log-colored plot).

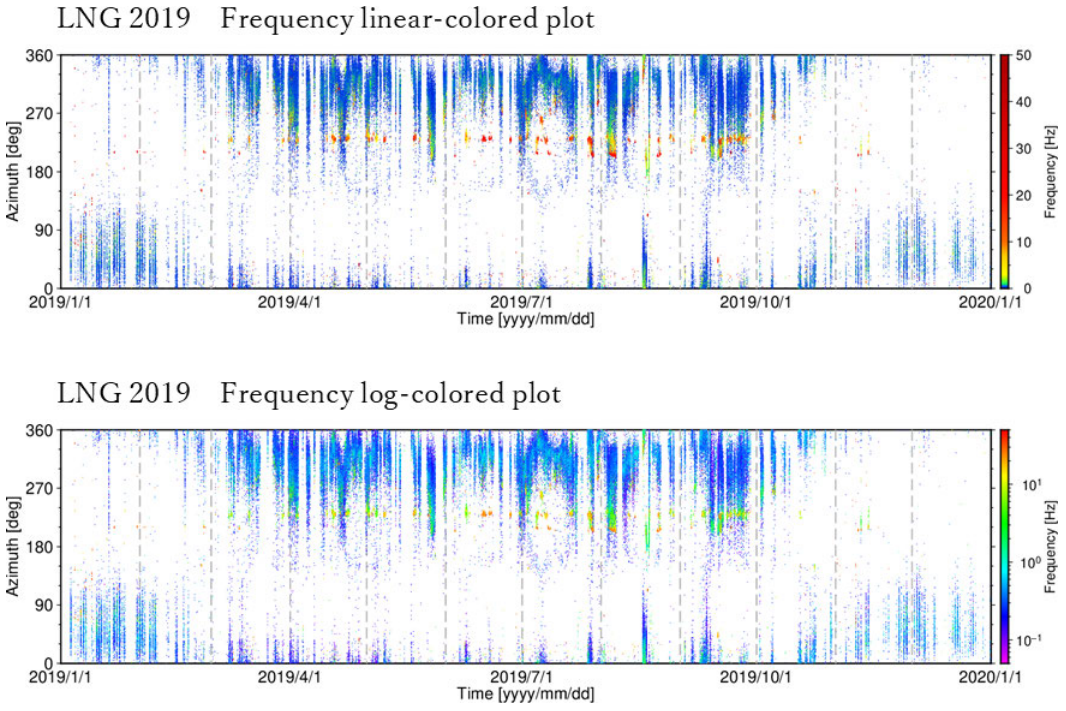

Figure 3b. Time sequence of azimuthal variation in arrival orientation and frequency contents of the detected infrasound signals by PMCC analysis (from January 01 to December 31, 2019, represented by a single year panel). The vertical axis for each panel indicates the back-azimuth (station-to-source) directions for LNG array. Colored bars representing in right hand side for each panel correspond to the central frequency [Hz] for each detected source event (upper; linear-colored plot, lower; log-colored plot).

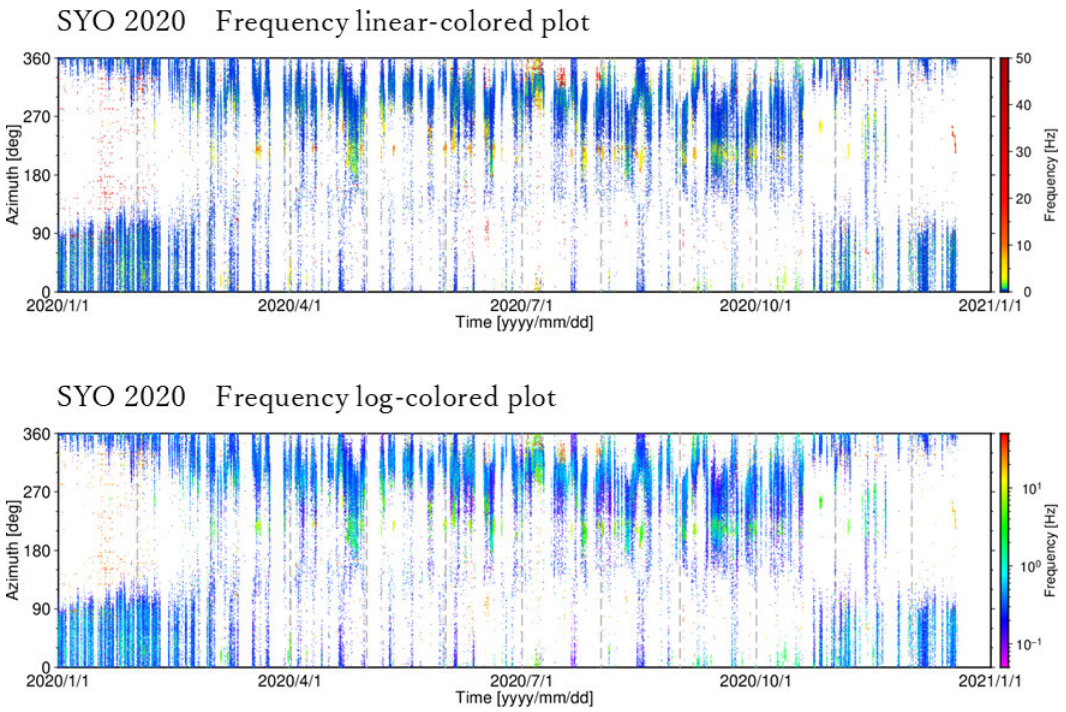

Figure 4a. Time sequence of azimuthal variation in arrival orientation and frequency contents of the detected infrasound signals by PMCC analysis (from January 01 to December 31, 2020, represented by a single year panel). The vertical axis for each panel indicates the back-azimuth (station-to-source) directions for SYO array. Colored bars representing in right hand side for each panel correspond to the central frequency [Hz] for each detected source event (upper; linear-colored plot, lower; log-colored plot).

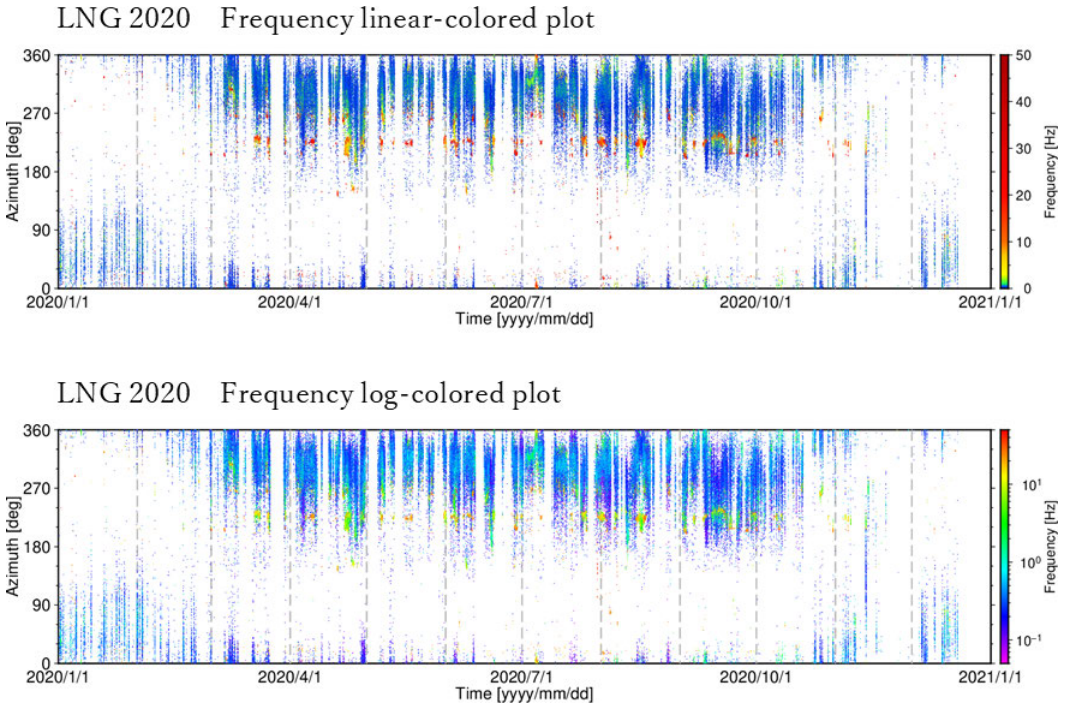

Figure 4b. Time sequence of azimuthal variation in arrival orientation and frequency contents of the detected infrasound signals by PMCC analysis (from January 01 to December 31, 2020, represented by a single year panel). The vertical axis for each panel indicates the back-azimuth (station-to-source) directions for LNG array. Colored bars representing in right hand side for each panel correspond to the central frequency [Hz] for each detected source event (upper; linear-colored plot, lower; log-colored plot).

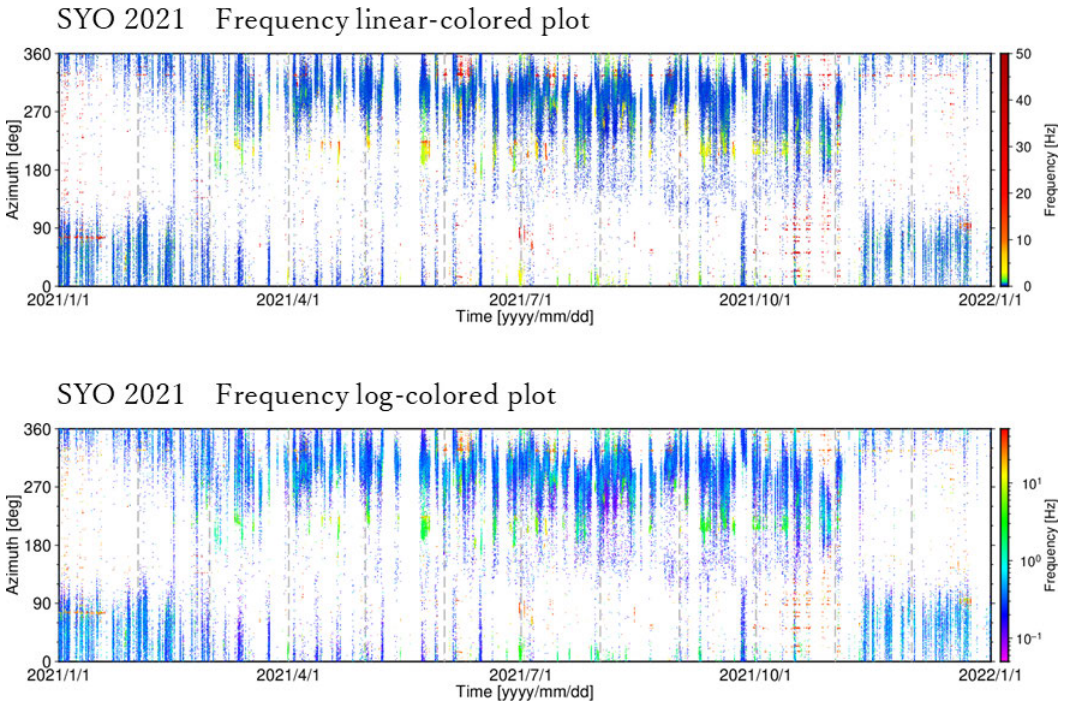

Figure 5a. Time sequence of azimuthal variation in arrival orientation and frequency contents of the detected infrasound signals by PMCC analysis (from January 01 to December 31, 2021, represented by a single year panel). The vertical axis for each panel indicates the back-azimuth (station-to-source) directions for SYO array. Colored bars representing in right hand side for each panel correspond to the central frequency [Hz] for each detected source event (upper; linear-colored plot, lower; log-colored plot).

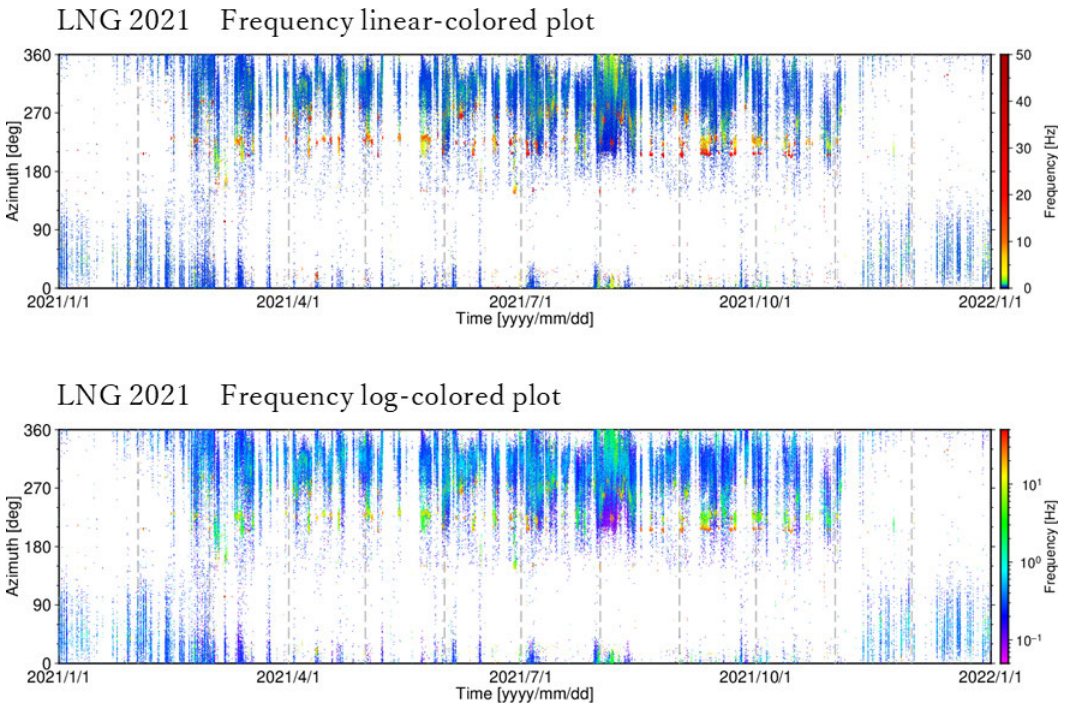

Figure 5b. Time sequence of azimuthal variation in arrival orientation and frequency contents of the detected infrasound signals by PMCC analysis (from January 01 to December 31, 2021, represented by a single year panel). The vertical axis for each panel indicates the back-azimuth (station-to-source) directions for LNG array. Colored bars representing in right hand side for each panel correspond to the central frequency [Hz] for each detected source event (upper; linear-colored plot, lower; log-colored plot).

A series of infrasound events with high frequency content and different orientations were detected with waveforms of short time duration during time periods in 2019-2021. Figure 6 documents the time sequence of azimuthal variation in arrival orientation and frequency contents for the detected infrasound signals for the month of July 2019 (upper panel). Configuration of the figure axis and notations are the same as Figs. 3-5. The red open square highlight detections on July 6-9, when characteristic infrasound events were identified around two distinct back-azimuths from the northwest and the southwest.

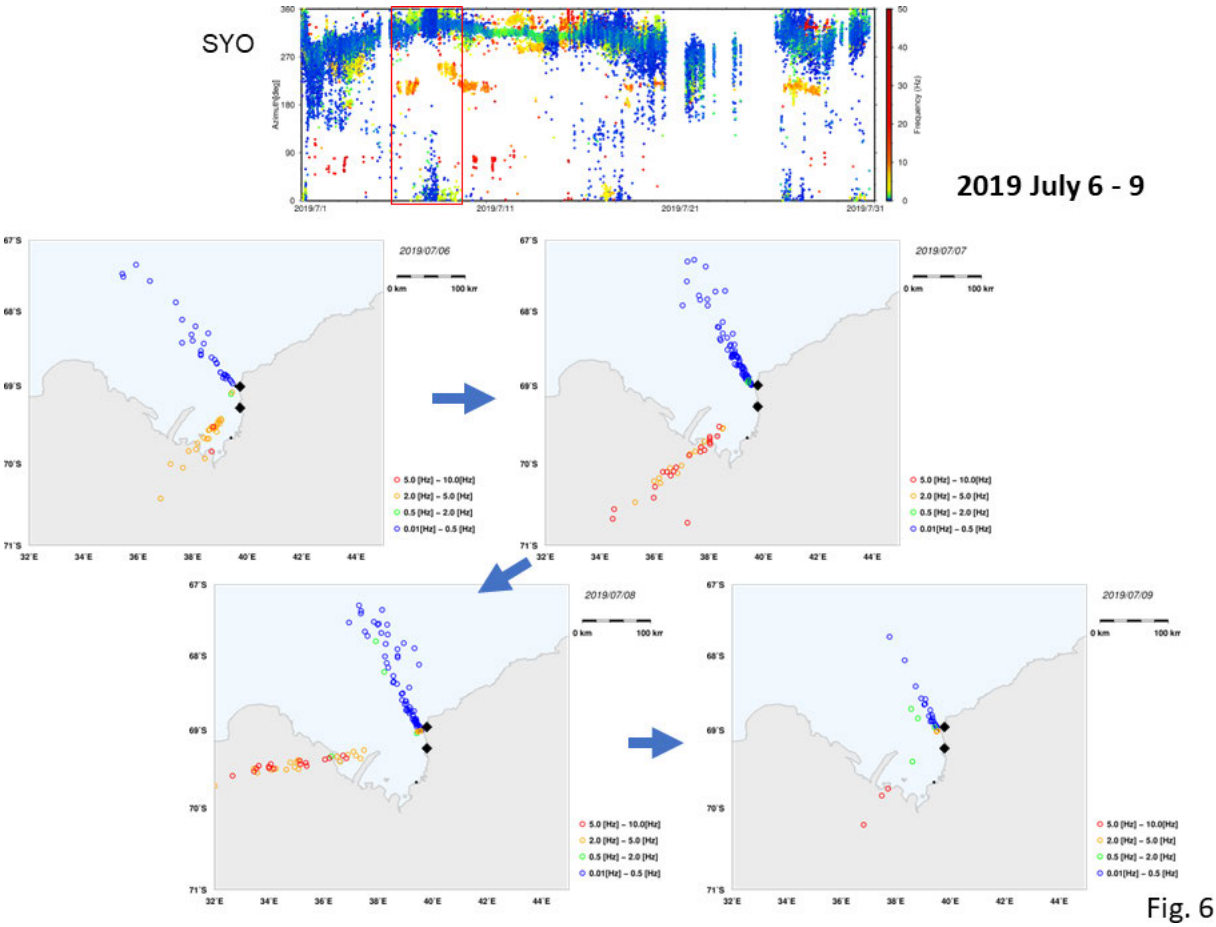

Figure 6. (upper panel) Time sequence of azimuthal variation in arrival orientation and frequency contents of detected signals by PMCC analysis for the one month of July 2019 (SYO). Red open squares correspond to the dates on July 6-9, when characteristic infrasound events were identified from different back-azimuths. (lower panel) Estimated source locations and their spatial migration of infrasound excitation on July 6-9, 2019, using two arrays of SYO and LNG. Black diamonds are infrasound stations in LHB. Estimated source locations are colored according to frequency contents of the wavelets by [Hz].

The lower panel of Fig. 6 contains the estimated infrasound source locations and their spatial migration on July 6-9, 2019, using the two arrays SYO and LNG. Black diamonds are infrasound stations in LHB. Estimated source locations are colored according to frequency contents of the wavelets by [Hz]. Relatively low frequency content waves (0.1-1.0 Hz) come from the northwest direction, while high frequency content waves (1.0-10 Hz) come from the southwest direction, with some fluctuation in backazimuths.

Figure 7a displays the estimated locations of infrasound sources from the northwest (low frequency events by 0.1-1.0 Hz bandpass filtered; blue colored open circles in the left panel) and associated waveform data for the two arrays SYO and LNG on July 7, 2019. The waveforms are believed to include contributions from microbaroms and their associated sea-ices dynamics related signals.

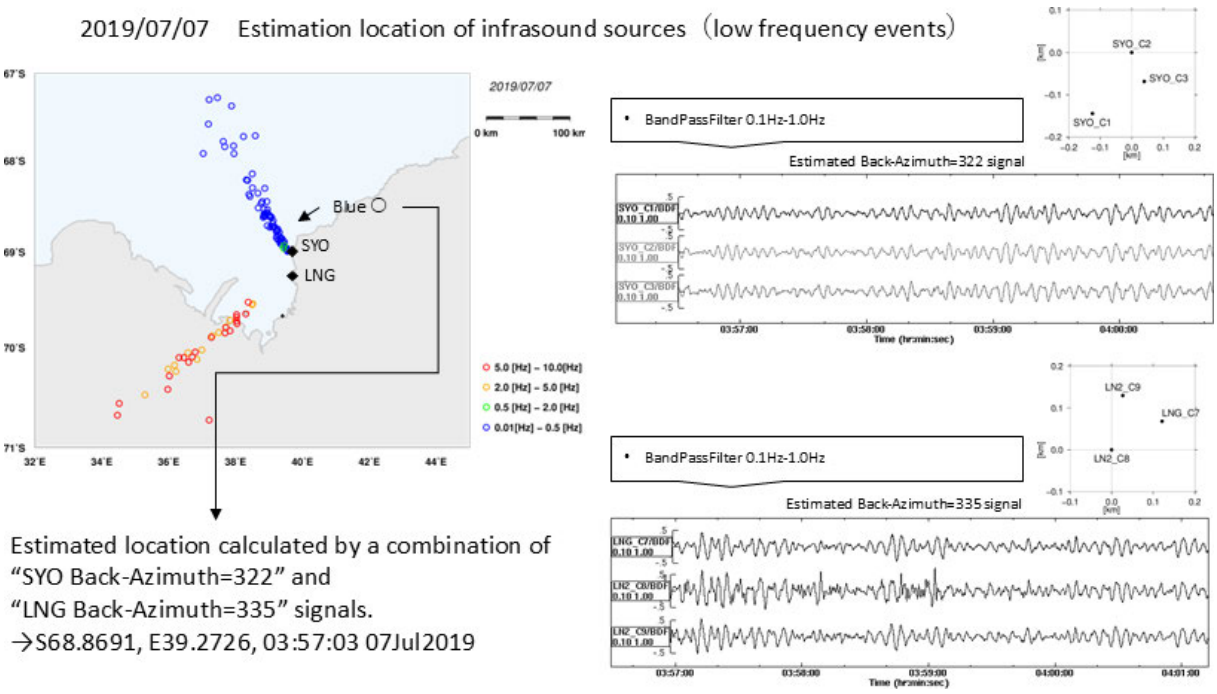

Figure 7a. Estimated location of infrasound sources from northwest direction (low frequency events by 0.1-1.0 Hz bandpass filtered; blue colored open circles in the left panel) and waveform data from SYO and LNG on July 7, 2019. The signals are estimated to include a component of microbaroms and their associated sea-ices dynamics related signals.

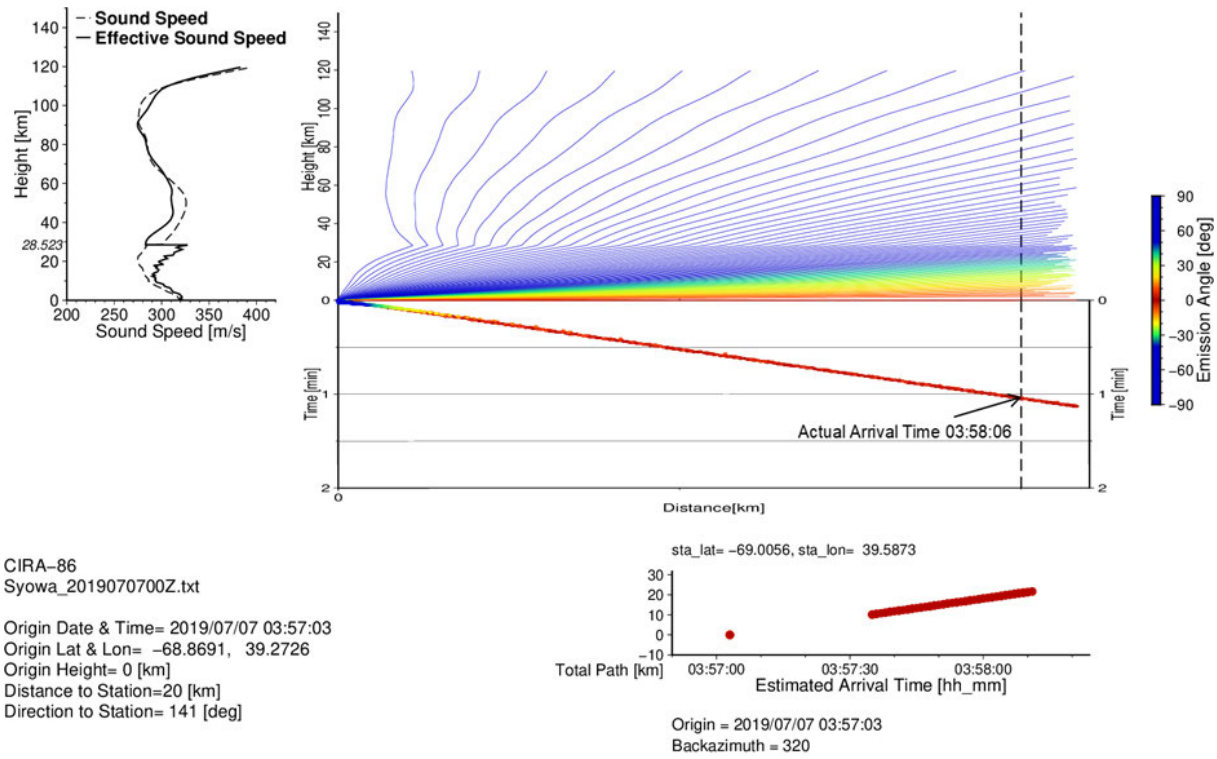

Figure 7b. Ray tracing results for the events of Fig. 7a to the SYO array, with an assumed atmosphere model that combines the upper air meteorological observation data from the Syowa Station (up to approximately 31 km in altitude) and climatological model from CIRA-86 (for altitudes between 30 km and 120 km). The estimated arrival times show the ray tracing calculation for the SYO array (right lower panel) are coincident with the arrival times observed in the actual waveforms (Fig. 7a).

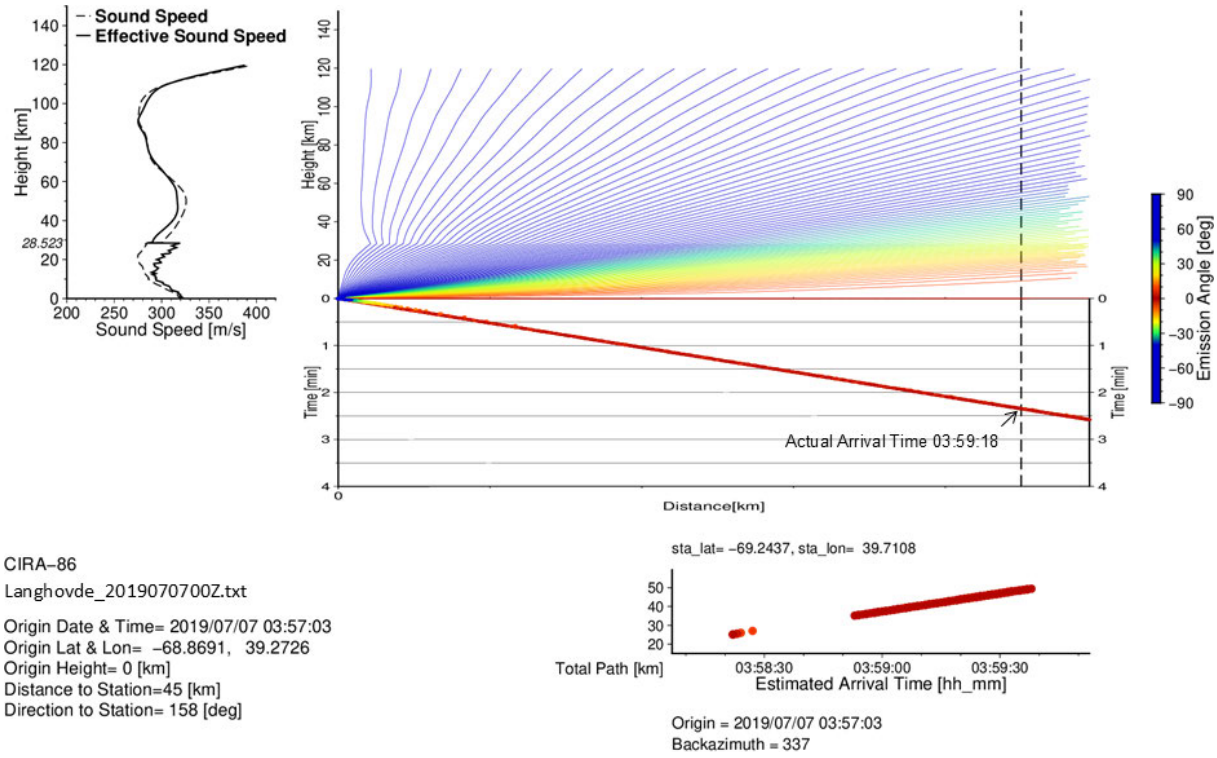

Figure 7c. The same ray tracing image as of Fig. 7b, but for the LNG array. The estimated arrival times from ray tracing (right lower panel) match well the observed arrival times (Fig. 7a).

Ray tracing results for the events in Fig. 7a to SYO and LNG arrays are shown in Figs. 7b and 7c, respectively. In the calculation of the ray propagation, we used an atmosphere model that combined the upper air meteorological observation data from the Syowa Station (up to approximately 31 km in altitude) and the climatological values based on the COSPAR International Reference Atmosphere (CIRA-86; https://www.aparc-climate.org/data-centre/data-access/reference-climatology/cira-86/) for the altitude ranges between 30 km and 120 km. The estimated arrival times by the ray tracing calculation for the two arrays coincide well with the arrival times observed in the actual waveforms (Fig. 7a).

In the same manner, estimated location of infrasound sources from southwest direction (high frequency events by 1.0-10 Hz bandpass filtered; green colored open circles in the left panel) and their waveforms for two arrays of SYO and LNG on July 9, 2019 are shown in Fig. 8a. The signals are estimated to be associated with cryosphere dynamics on the southern part of LHB. Ray tracing results for the events in Fig. 8a to both the arrays are illustrated in Fig. 8b. Estimated arrival times from the ray tracing for both the arrays coincident well with the observed arrival times (Fig. 8a).

Microbaroms included in seconds of data vary both in amplitude and frequency content in the relatively long period waveforms. These variations may correspond to local/regional atmospheric conditions, which are related to prevailing winds. Infrasound signals below 3 Hz frequency content are believed to be associated with "microbaroms" which can be excited by storms (Ishihara et al., 2015; 2020; Murayama et al., 2017b). Based on frequency content and source locations, infrasound events form northwest direction are identified as "microbaroms" from the Bay and are accompanied by a relatively low frequency content. In contrast, the source events from southwest direction have a higher frequency content and presumably involve more impulsive cryosphere dynamics in the Bay, especially relating to the dynamics of glaciers and ice-streams in the southern coastal area of LHB.

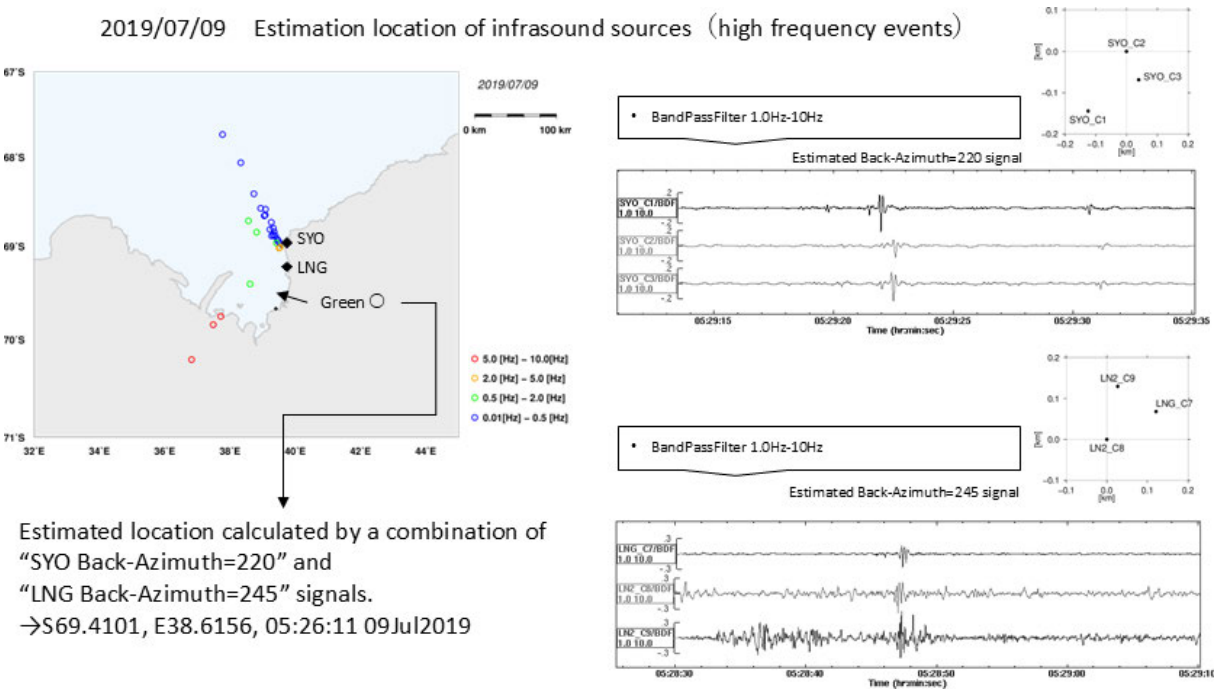

Figure 8a. Estimated location of infrasound sources from southwest direction (high frequency events by 1.0-10 Hz bandpass filtered; green colored open circles in the left panel) and associated waveforms for SYO and LNG on July 9, 2019. The signals are estimated to be associated with cryosphere dynamics on the southern part of LHB.

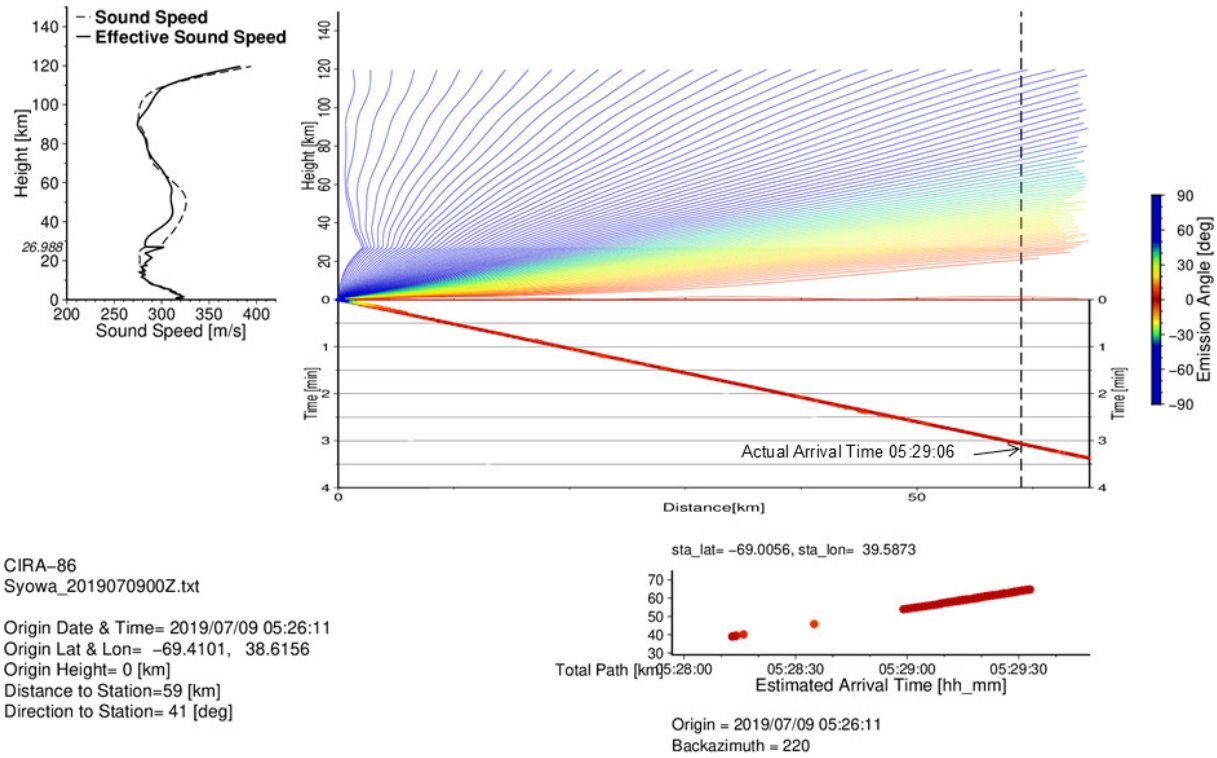

Figure 8b. Ray tracing results for the events in Fig. 8a to SYO using an atmospheric model that combines the upper air meteorological observation data from the Syowa Station (up to approximately 31 km in altitude) and climatological estimates from CIRA-86 (for altitudes between 30 km and 120 km). The estimated ray tracing arrival times for SYO (right lower panel) are coincide well with observed arrival times (Fig. 8a).

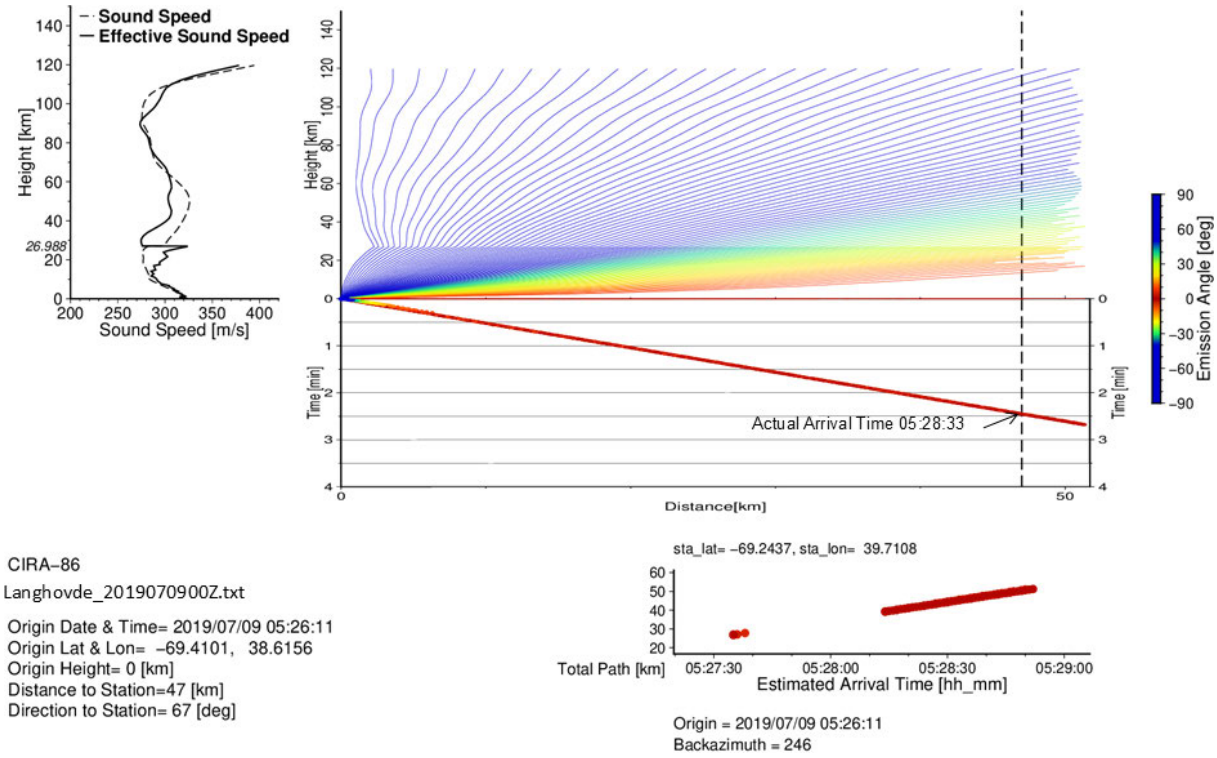

Figure 8c. The same ray tracing image as Fig. 8b, but for LNG. Estimated ray tracing arrival times for LNG (right lower panel) well match the observed arrival times (Fig. 8a).

4. Estimation result of source locations

Several interesting features of the estimated source locations were determined from the three years of data as shown in Figs. 9a-9c. Infrasound signals below 3 Hz frequency (mostly represented by "blue color") propagate from sources to the arrays in the north-northeast direction during the "autumn" season in southern hemisphere (i.e, from January to April). However, it appears that the propagation directions gradually changes to the northwest-west after February. After October until the next austral summer seasons, propagation direction return to the north-northeast direction. These low frequency signals below the 3 Hz appear as continuous time series observed across the three years of data. These signals are assumed to be influenced by the "time varying winds" and "oceanic swells". These migrating propagating directions were identified in previous array results (Murayama et al., 2017b; 2023).

A second characteristic feature of the infrasound signals below 3 Hz is that they propagate in north-northeast direction during "autumn" season (i.e., from January to April; and from October to the next summer). These signals might be generated by "katabatic wind" along the westward dipping slope of the continental ice sheet (Kikuchi and Ageta, 1989; Ishikawa et al., 1996).

The infrasound signals migrate to the northwest-west after February and could be related to the sources in the Bay. These infrasound signals are characterized as "microbaroms" which can be excited by nearby storms and associated oceanic swells. It is also possible that the signals contain associated dynamic signals caused by collisions between sea-ices, icebergs inside the Bay overlapping with the microbaroms (Murayama et al., 2017a; 2017b; 2018; 2023). The microbaroms signals were not adequately observed during the extreme stormy conditions with wind speeds over 15 m/s. Distinguishing the signals from the two effects of "katabatic wind" and "microbaroms" is difficult based only on their frequency content. However, the source orientations from the east and northeast directions correspond to the Antarctic continent; favoring infrasound generation by "katabatic wind".

Third, sporadic occurrences of infrasound signals with frequencies over 4 Hz appeared to propagate from about 200°during all seasons, particularly during clear conditions in winter season. These 4 Hz signals are observed at similar locations as the signals below 3 Hz. These higher frequency signals might be due to cryosphere dynamics, at the same time as signals generated by oceanic swells excited by storms. The high frequency waves come from the southwest which corresponds to the inside of Bay, where several geomorphological scale glaciers/ice streams

are embedded along the coasts of LHB, surrounded by the sea-ice inside the Bay. High frequency infrasound signals are particularly apparent in July 2019 (Fig. 6).

Finally, high frequency signals above 6 Hz are observed from locations near SYO in January to mid-February. The signals may be attributed to helicopters transporting supplies from the icebreaker vessel "Shirase" and the Syowa Station. Expedition members and the icebreaker vessel "Shirase" were near SYO during the time period of austral summer. This interpretation is strengthened by the evidence that these characteristic signals were not recorded during the winter season at either SYO or LNG, as well as no appearance in the data at S16 array (over the continental ice sheet about 15 km eastward apart from SYO) during the whole season in 2015 (lower panel of Fig. 3 in Murayama et al., 2015).

5. Discussion

In order to compare the infrasound observation with the other environmental datasets around LHB, the MODIS satellite monthly images for the whole season in 2019-2021 were investigated (Figs 10a-10c). Data were analyzed except time periods when the study area was either covered with clouds or during the dark season in Antarctica (i.e., May-August). Infrasound source locations using SYO and LNG for three years are plotted in Figs. 9a-9c illustrating the northern edges of the fast-sea-ice covering over the Bay (i.e., the northwest-north directions from the two arrays) as well as the area near the outlet glaciers at the southern part of LHB (i.e., the southeastern direction from the two arrays).

Most of the infrasound sources were located to the northwest of the LHB (Figs. 10a-10c), extending toward the Sothern Indian Ocean. The majority of these events are concentrated in the area and on the edges of the fast-sea-ices, as well as the icebergs and the pack-ice area where cryospheric dynamic movements (crashing, collision, break-off, etc.) involving oceanic swells and/or storms were presumably generating the infrasound sources.

Other geophysical observations, such as seismic, geodetic, geomagnetic observations, are expected to document the characteristic dynamics of the solid earth response in terms of relationship with other spheres including

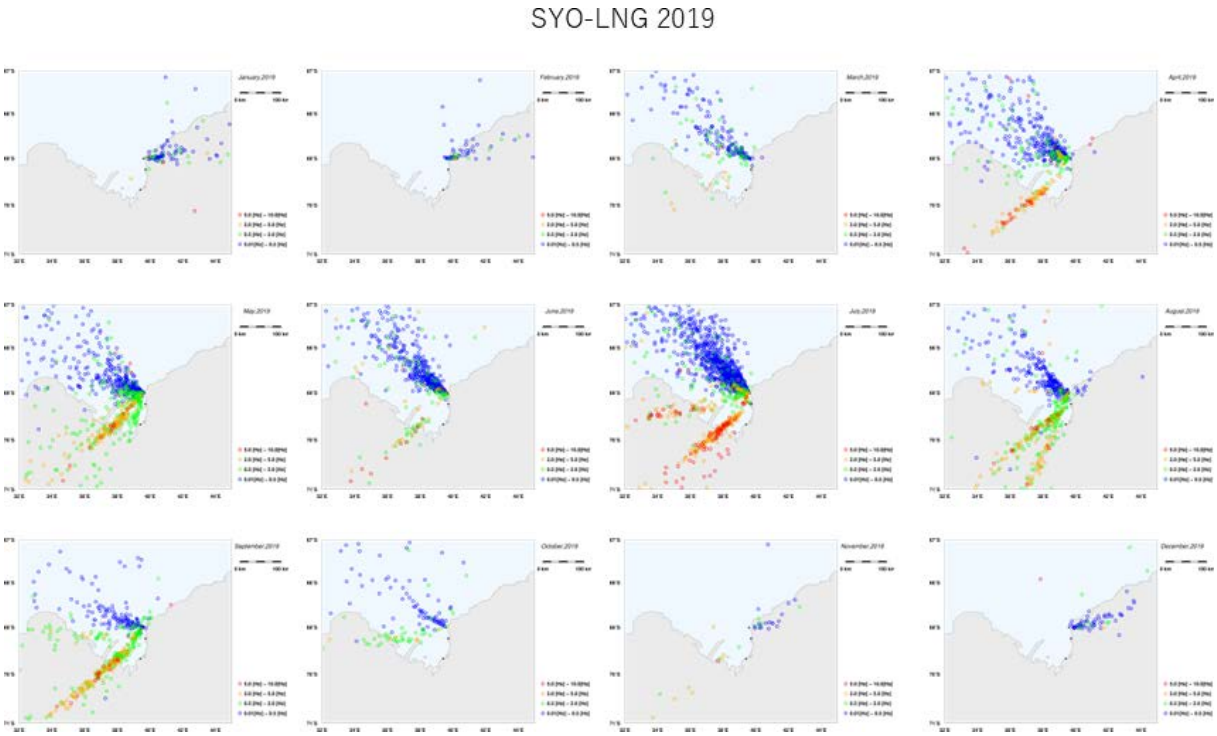

Figure 9a. Distribution of the source locations of the detected infrasound signals by PMCC analysis (from January 01 to December 31, 2019, represented by separated panel for one month), combined by both the SYO and LNG arrays. Colors representing in right hand side for each panel correspond to the central frequency [Hz] for each detected source event.

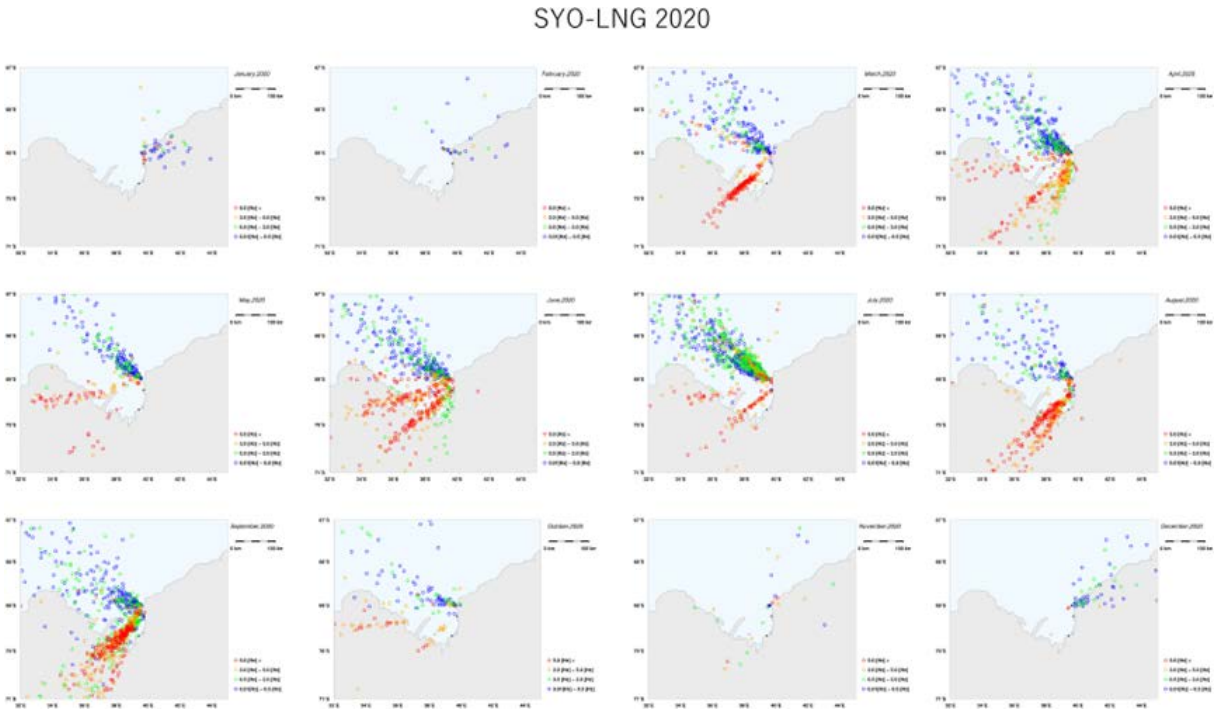

Figure 9b. Distribution of the source locations of the detected infrasound signals by PMCC analysis (from January 01 to December 31, 2020, represented by separated panel for one month), combined by both the SYO and LNG arrays. Colors representing in right hand side for each panel correspond to the central frequency [Hz] for each detected source event.

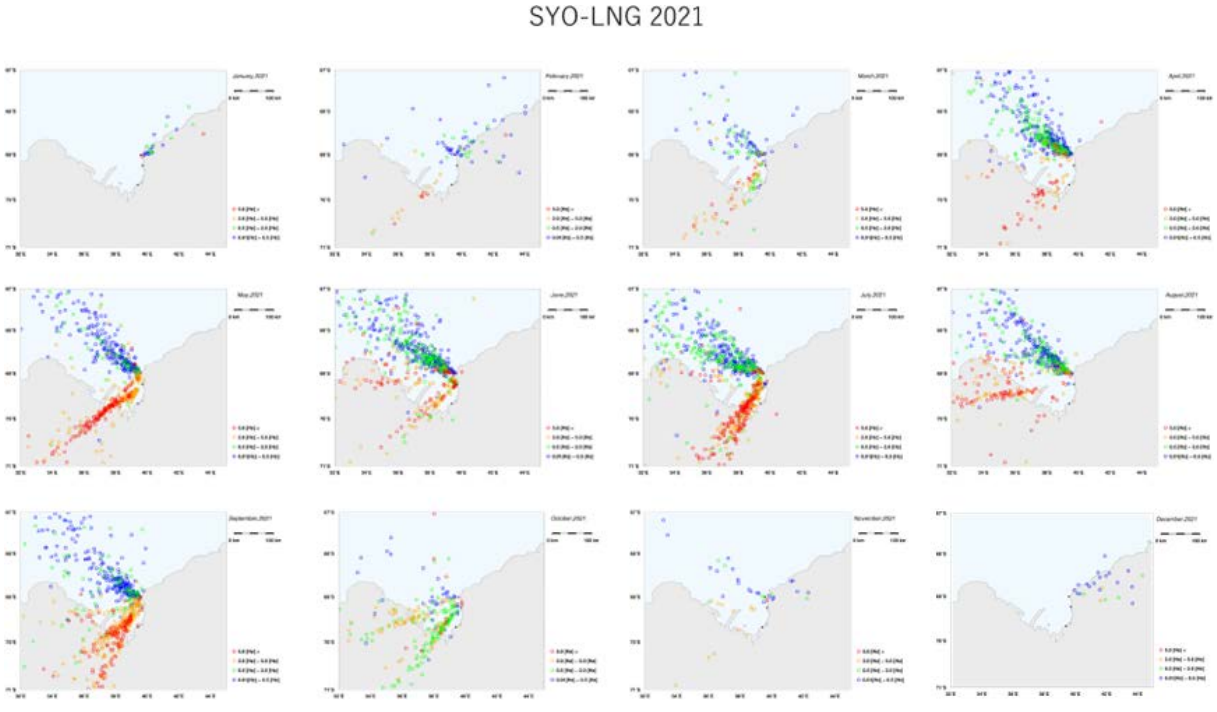

Figure 9c. Distribution of the source locations of the detected infrasound signals by PMCC analysis (from January 01 to December 31, 2021, represented by separated panel for one month), combined by both the SYO and LNG arrays. Colors representing in right hand side for each panel correspond to the central frequency [Hz] for each detected source event.

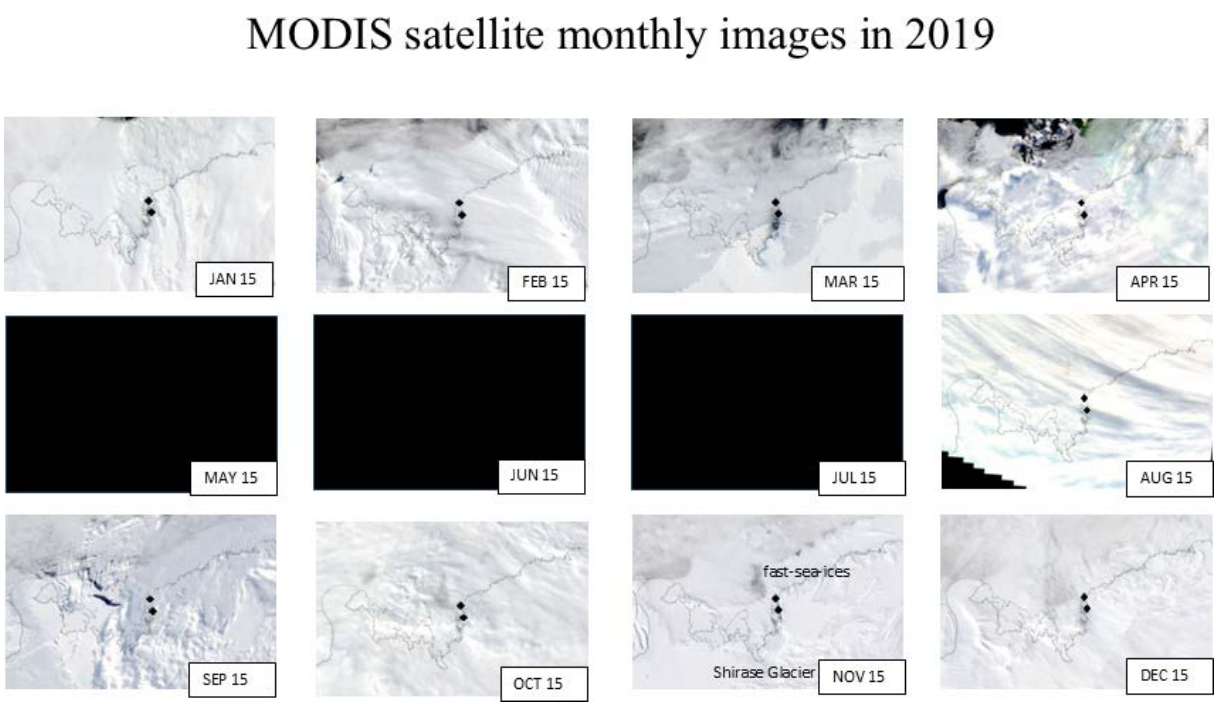

Figure 10a. MODIS satellite monthly images on each 15th day around LHB in 2019. The locations of SYO and LNG are shown by black solid squares (diamonds).

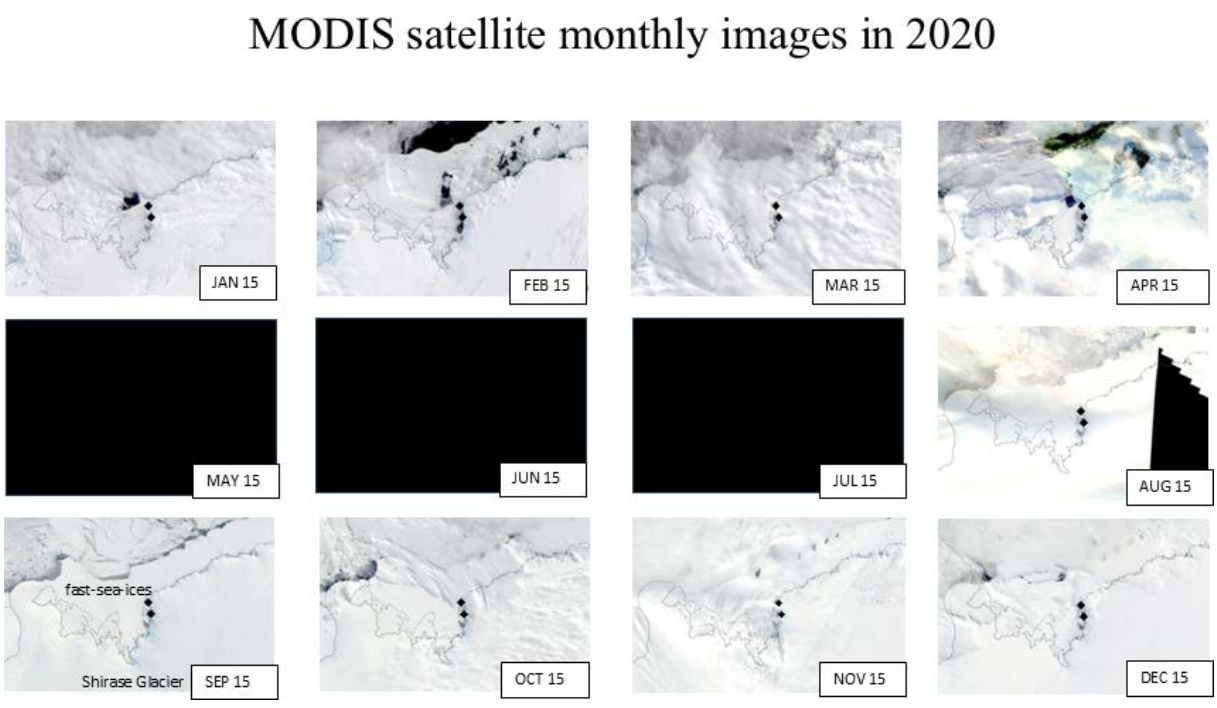

Figure 10b. MODIS satellite monthly images on each 15th day around LHB in 2020. The locations of SYO and LNG are shown by black solid squares (diamonds).

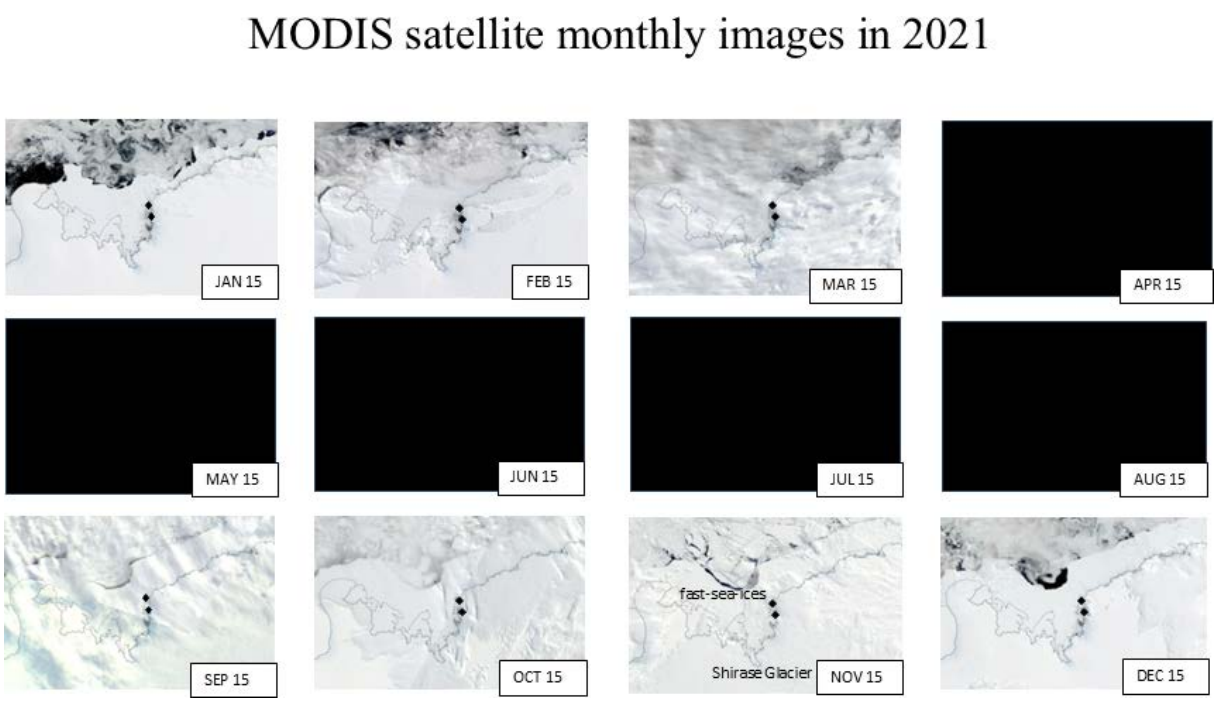

Figure 10c. MODIS satellite monthly images on each 15th day around LHB in 2021. The locations of SYO and LNG are shown by black solid squares (diamonds).

cryosphere (Kanao et al., 2011; Kanao et al., 2012). In contrast, the infrasound measures atmosphere waves generated near the surface as a result of interactions between surrounding environments which contain ocean, solid earth and cryosphere dynamics as well as atmospheric propagation. Therefore, infrasound data is expected to constrain physical processes between the spheres with physical interpretations improved using other datasets to reveal multi-sphere interaction in polar regions. Seasonal variations of microbaroms amplitude are expected, if they are generated by processes producing microseisms (Grob et al., 2011). The seasonal variations in microseisms have been found to depend on sea-ice extent/volume surrounding the LHB, which impede both direct ocean-to-continent coupling and coastal reflection (Kanao et al., 2012). Continuous monitoring of infrasound in LHB over multiple years will add to constraining these effects.

The infrasound array alignment at SYO and LNG in LHB made it possible to quantify arrival direction of infrasound excitation sources. The precise location of the sources might be compared with those obtained by seismological approaches in the future. It may also useful to compare these signals with other data, such as hydro-acoustics that share sensitivity over part of the infrasound frequency ranges (Hanson et al., 2001).

6. Conclusion

Time-space variability of source locations from infrasound waves covering three years, 2019-2021, was investigated by analyzing data from two tripartite arrays deployed on coastal outcrops in LHB, Antarctica. A number of infrasound sources were detected and found to be located between north and north-west from the arrays. Many of these events are generated within the Southern Indian Ocean and the northern part of LHB with frequency content of a few seconds and conclude to be “microbaroms” generated by oceanic swells. During austral summer to fall seasons, a majority of infrasound sources are from the north-east. These sources may be related to the interaction of katabatic winds with the continental coastal area. Furthermore, several sporadic infrasound events occur during the winter with predominantly higher frequency content of over 3 Hz, compared to the lower frequency microbaroms. On the basis of a comparison with sea-ices and glacier distribution from MODIS satellite images, the candidates of these sporadic high-frequency sources are suggested to be associated with cryosphere dynamics in LHB. This study suggests that continuous monitoring of infrasound could be a new proxy for characterizing the surface environment and temporal climate change in the Antarctic.

Acknowledgements. The authors express their sincere appreciation to many people who dedicatedly collaborated in the infrasound observations at LHB, especially the related members of the Japanese Antarctic Research Expeditions (JARE). The authors also express acknowledgements to the National Aeronautics and Space Administration (NASA) for the use of MODIS images. This work was partially supported by JSPS KAKENHI Grant Number 26241010 (P.I. by Dr. Masaki Kanao). They also express appreciation to the editorial office and reviewers for their editorial endeavors and critical review comments for publishing this article.

References

Arai, N., M. Iwakuni, S. Watada, Y. Imanishi et al. (2011). Atmospheric boundary waves excited by the tsunami generation related to the 2011 great Tohoku-Oki earthquake, Geophys. Res. Lett. 38, L00G18, doi:10.1029/2011GL049146.

Arrowsmith, S. J., D. O. ReVelle, W. N. Edwards and P. Brown (2008). Global Infrasonic Signals from Three Large Bolides, Earth, Moon and Planets 102, 357-363.

Cansi, Y. (1995). An automatic seismic event processing for detection and location: The P.M.C.C. Method, Geophys. Res. Lett., 22, 1021-1024.

Cansi, Y. and Y. Klinger (1997). An automated data processing method for mini-arrays, CSEM/EMSC European-Mediterranean Seismological Centre, News Lett., 11, 1021-1024.

Grob, M., A. Maggi and E. Stutzmann (2011). Observations of the seasonality of the Antarctic microseismic signal, and its association to sea ice variability, Geophys. Res. Lett., 38, L11302, doi:10.1029/2011GL047525.

Hanson, J., R. L. Bras, D. Brumbaugh, J. Guern et al. (2001). Operational Processing of Hydroacoustics at the Prototype International Data Center, Monitoring the Comprehensive Nuclear-Test-Ban Treaty: Hydroacoustics, Pageoph Topical Volumes, 2001, 425-456.

Hedlin, M., M. Garces, H. Bass, C. Hayward et al. (2002). Listening to the secret sounds of Earth's atmosphere, Eos Trans., AGU, 83, 557, 564-565.

Hedlin, M. and B. Alcoverro (2005). The use of impedance matching capillaries for reducing resonance in rosette infrasonic spatial filters, J. Acoust. Soc. Am., 117, 1880-1888.

Ishikawa, T., J. Ukita, K. I. Oshima, M. Wakatsuchi et al. (1996). Coastal polynyas off East Queen Maud Land observed from NOAA AVHRR data, J. Oceanography, 52, 389-398.

Ishihara, Y., M. Kanao, M.-Y. Yamamoto, S. Toda et al. (2015). Infrasound observations at Syowa Station, East Antarctica: Implications for detecting the surface environmental variations in the polar regions, Geosci. Front., 6, 285-296.

Ishihara, Y., T. Murayama, M.-Y. Yamamoto, T. Matsushima et al. (2020). Infrasound observation at Japanese Antarctic Station Syowa:11 years observations and results, Polar Data J., 4, 45-54, doi:10.20575/00000012.

Iyemori, T., M. Nose, D. S. Han, Y. Gao et al. (2005). Geomagnetic pulsations caused by the Sumatra earthquake on December 26, 2004, Geophys. Res. Lett., 32, L20807, doi:10.1029/2005GL024083.

Kanao, M., Y. Usui, T. Inoue and A. Yamada (2011). Broadband seismic deployments for imaging the upper mantle structure in the Lützow-Holm Bay region, East Antarctica, Inter. J. Geophys., 2011, 1-15, doi:10.1155/2011/272646.

Kanao, M., A. Maggi, Y. Ishihara, M.-Y. Yamamoto et al. (2012). Interaction on Seismic Waves between Atmosphere - Ocean - Cryosphere and Geosphere in Polar Region, In: Kanao, M., H. Takenaka, Y. Murai, J. Matsushima and G. Toyokuni (Eds.), Seismic Waves – Research and Analysis –, ISBN 978-953-307-944-8, InTech. Publisher, Rijeka, Croatia, 1-20.

Kikuchi, T and Y. Ageta (1989). A preliminary estimate of inertia effects in a bulk model of katabatic wind, Proc. NIPR Symp. Polar Meteorol. Glaciol., 2, 61-69.

Matoza, R. S., M. A. H. Hedlin and M. A. Garces (2007). An infrasound array study of Mount St. Helens, J. Volcanol. Geotherm. Res., 160, 249-262.

Murayama, T., M. Kanao, M.-Y. Yamamoto, Y. Ishihara et al. (2015). Infrasound Array Observations in the Lützow-Holm Bay region, East Antarctica, Polar Sci., 9, 35-50, 10.1016/j.polar.2014.07.005.

Murayama, T., M. Kanao, M.-Y. Yamamoto and Y. Ishihara (2017a). Infrasound signals and their source location inferred from array deployment in the Lützow-Holm Bay region, East Antarctica: 2015 January-June, Inter. J. Geosci., 8, 181-188, doi:10.4236/ijg.2017.82007.

Murayama, T., M. Kanao, M.-Y. Yamamoto, Y. Ishihara et al. (2017b). Time-space variations of infrasound sources related to environmental dynamics around the Lützow-Holm Bay, East Antarctica, Polar Sci., 14, 39-48, doi:10.1016/j.polar.2017.10.001.

Murayama, T., M. Kanao and M.-Y. Yamamoto (2018). Characteristic infrasound events associated with sea-ice discharges in the Lützow-Holm Bay of Antarctica: April 2016, Special Issue on "Antarctica – A Key To Global Change", IntechOpen, London, United Kingdom, 1-10, doi:10.5772/intechopen.83023.

Murayama, T., M. Kanao and M.-Y. Yamamoto (2023). Migration of source locations and arrival orientations for infrasound excitation in the Lützow-Holm Bay, Antarctica: January-April 2017, InfraMatics, 4, 1, 1-10, doi:10.4236/inframatics.2023.41001.

Podolskiy, E. A., R. Genco, S. Sugiyama, F. Walter et al. (2017). Seismic and infrasound monitoring of Bowdoin Glacier, Greenland, Low Temperature Science, 75, 15-36, doi:10.14943/lowtemsci.75.15.

Walker, K. T. and M. A. H. Hedlin (2010). A Review of Wind-Noise Reduction Methodologies, In: Pichon, A. L., E. Blanc and A. Hauchecorne (Eds.), Infrasound Monitoring for Atmospheric Studies, Springer Science + Business Media B.V., Chapter 5, 141-182, doi:10.1007/978-1-4020-9508-5.

Wilson, C. R. (1969). Auroral infrasonic waves, J. Geophys. Res. 747, 1812-1836, doi:10.1029/JA074i007p01812.

Yamamoto, M.-Y., Y. Ishihara and M. Kanao (2013). Infrasonic waves in Antarctica: A new proxy for Monitoring Polar Environment, Inter. J. Geosci., 4, 797-802, https://www.scirp.org/journal/paperinformation?paperid=33486.

***CORRESPONDING AUTHOR: Masaki KANAO**,
National Institute of Polar Research, Research Organization of Information and Systems, Midori-cho, Tachikawa-shi, Tokyo
e-mail: kanao@nipr.ac.jp